

Supporting Material for: Assessing the accuracy of different solvation models to describe protein adsorption

Maria Ortega,[†] J. G. Vilhena,^{*,†,‡} Pamela Rubio-Pereda,^{¶,§} P. A. Serena,[¶] and Rubén Pérez^{*,†,||}

[†]*Departamento de Física Teórica de la Materia Condensada, Universidad Autónoma de Madrid, E-28049 Madrid, Spain*

[‡]*Department of Physics, University of Basel, Klingelbergstrasse 82, CH-4056 Basel, Switzerland*

[¶]*Instituto de Ciencia de Materiales de Madrid (ICMM), CSIC, c/ Sor Juana Ines de la Cruz 3, E-28049 Madrid, Spain*

[§]*Centro de Investigación Científica y de Educación Superior de Ensenada 3918, postal code 22860, Ensenada, Baja California, Mexico*

^{||}*Condensed Matter Physics Center (IFIMAC), Universidad Autónoma de Madrid, E-28049 Madrid, Spain*

E-mail: guilhermevilhena@gmail.com; ruben.perez@uam.es

January 25, 2019

1 Definition of the different energy-related magnitudes.

Here we explain the difference between the three energy-related magnitudes used in the manuscript: E_i , ΔE_i and $\Delta_t E_i$. The subindex i indicates that these three definitions can be applied to the different energy components that contribute to the adsorption process.

1. E_i corresponds to a given energy contribution.
2. ΔE_i describes the variation of a particular energy contribution (E_i) with the protein-surface distance during the adsorption process.
3. $\Delta_t E_i$ represents the variation of that energy contribution (E_i) during the time of adsorption.

2 FIGURES

2.2 SIMULATION METHODS

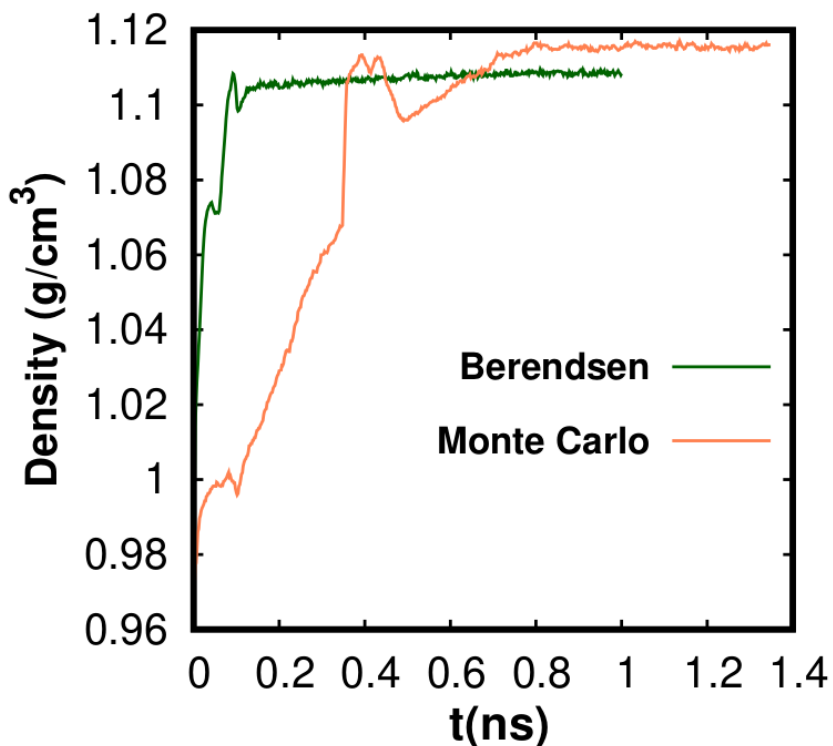


Figure S1: **Evolution of the system density during the preliminary NPT simulation used for equilibrate the volume of the system using two different barostats.** During this preliminary stage, we heat up the system from 0 to 300 K while restraining the position of the protein backbone and the first graphene layer. Here we compare the results obtained with two different barostats: Berendsen¹ (the one used in our adsorption protocol, green line) and Monte Carlo² (orange). The time evolution of the system density does depend on the barostat used, but the converged density value obtained at the end of the simulation (ρ) is roughly the same with the two barostats: $\rho_{Ber} = 1.1084 \text{ g/cm}^3$ and $\rho_{MC} = 1.1161 \text{ g/cm}^3$. This small difference between the two final value (less than 1%) confirms that, in spite of its known limitations,³ the Berendsen barostat is suitable for this task.

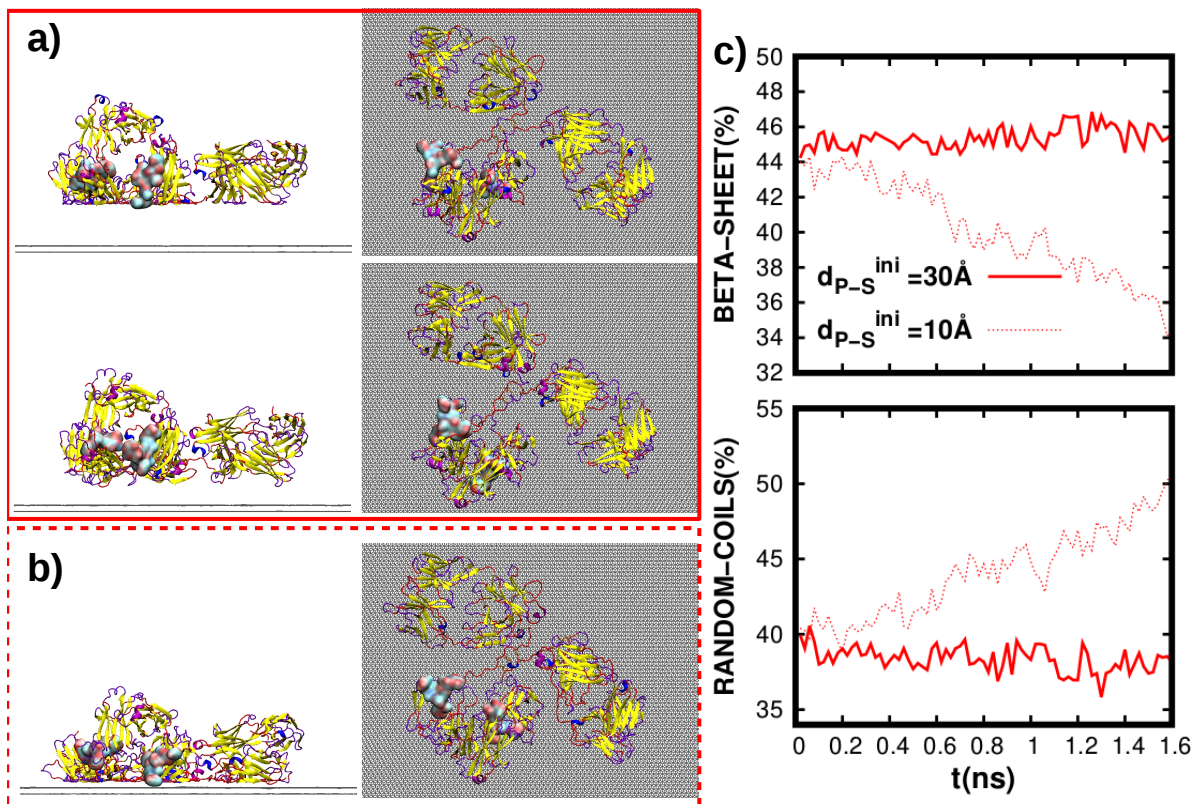


Figure S2: **Analysis of the possible structural changes that could be induced during the SMD simulation for restraining the C_α belonging to 16 cysteine residues.** To prove that restraining the C_α belonging to 16 cysteine residues does not affect the structure of the protein, we perform the same SMD simulation as in our adsorption protocol but starting from a larger protein-surface distance ($d_{p-s}^{ini} = 30 \text{ \AA}$). In this way, the protein does not interact with the substrate during the whole SMD process and the only possible cause for a structural protein distortion is the restraining of those 16 C_α carbons. We have used the OBC method,⁴ as this is the implicit solvent method which distorts more the protein structure during the adsorption process (see Fig. 2 of the main manuscript). Both side (left) and top (right) views of the initial (top) and final (bottom) configurations of this simulation are shown in **a)**. The color representation used for the protein-substrate system is the same as in Fig. 1 of the main manuscript. For comparison, we also include in **b)** the final configuration obtained after the SMD process of our OBC implicit solvent adsorption simulation, i.e. the one analyzed in the main manuscript ($d_{p-s}^{ini} = 10 \text{ \AA}$). In **c)**, the time evolution of the β -sheet (top) and random-coils (bottom) content of the IgG during both SMD processes, i.e. starting at $d_{p-s}^{ini} = 30 \text{ \AA}$ (continuous line) and at $d_{p-s}^{ini} = 10 \text{ \AA}$ (dashed line) is also shown. These results clearly show that, when the protein does not interact with the substrate, the secondary and tertiary structure of the IgG barely changes during the SMD process, confirming that the applied restrain is not affecting the IgG structural stability.

2.3 RESULTS AND DISCUSSION

2.3.1 Structural dynamics of the adsorption process: comparison between different solvent models

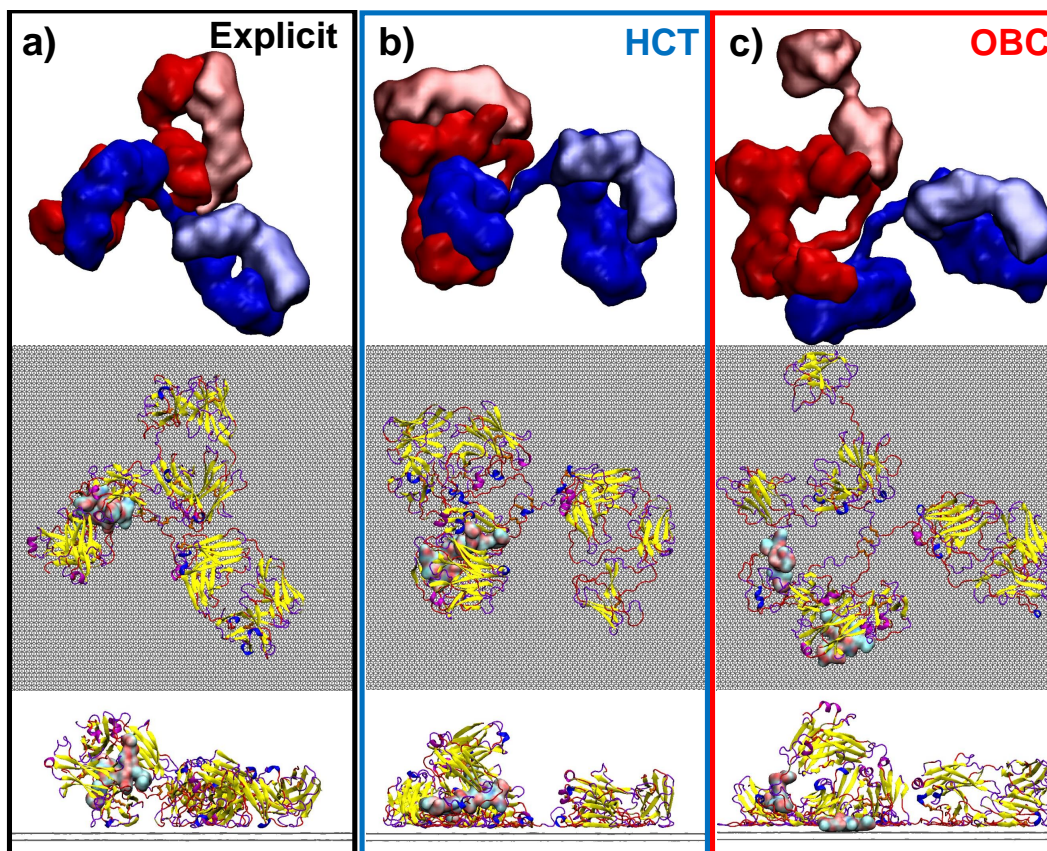


Figure S3: **Final IgG-graphene configurations obtained at the end of the adsorption process.** The final configurations obtained using **a)**Explicit TIP3P,⁵ **b)**HCT implicit⁶ and **c)**OBC implicit⁴ solvent methods are shown here. Both side (bottom row) and top views (middle row) of these configurations are displayed. The color representation used for the system protein-substrate is the same as in the Fig. 1 of the main manuscript. The relative configuration of the four chains⁷ that conforms the IgG upon adsorption is also shown (top row).

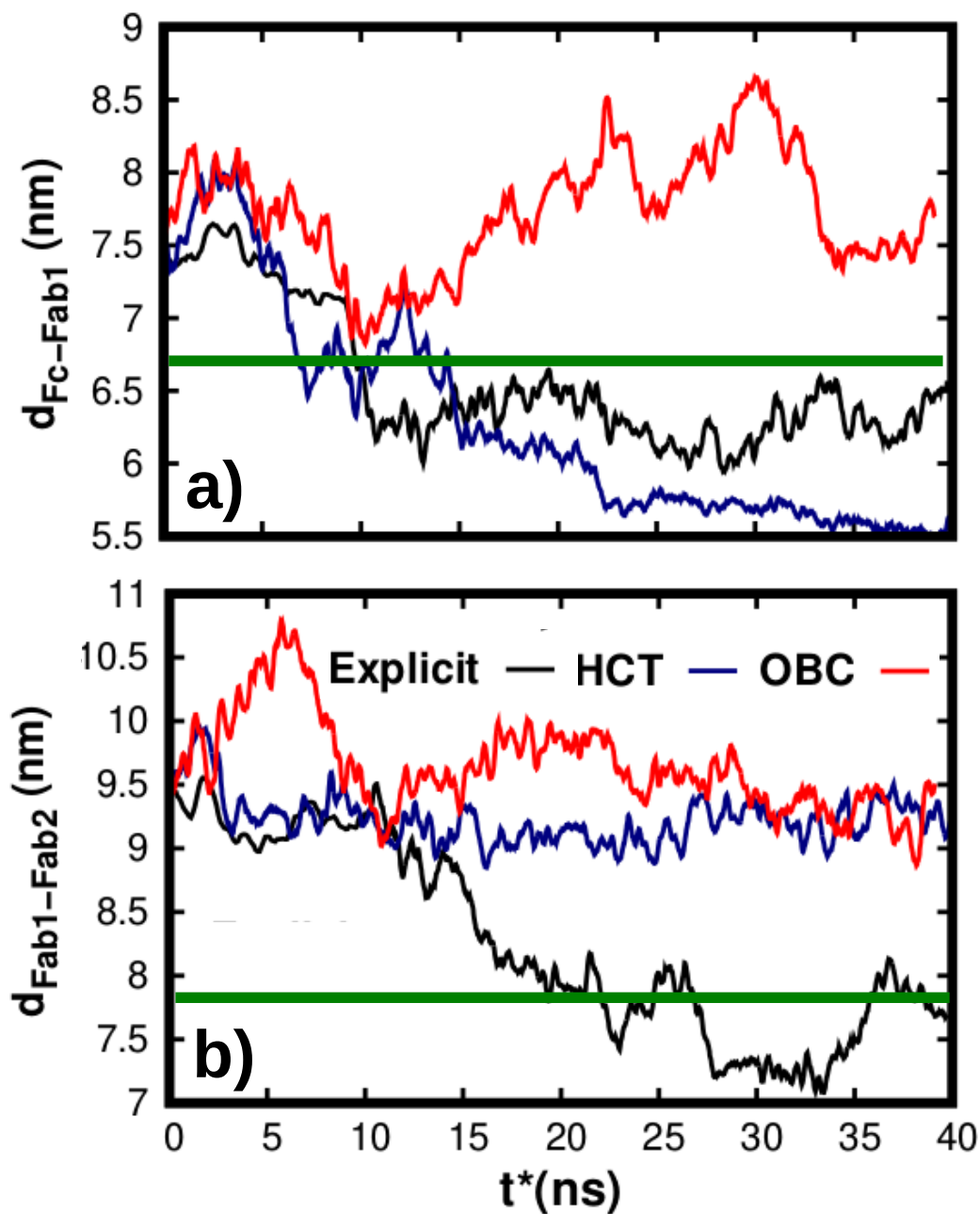


Figure S4: Time evolution of the inter-domain distances during the adsorption process. Here we show the evolution of the inter-domain distances **a)** $d_{Fc-Fab1}$ and **b)** $d_{Fab1-Fab2}$ using the three solvent methods here considered: Explicit⁵ (black), HCT implicit⁶ (blue) and OBC implicit⁴ (red). The experimental values of these two inter-domain distances, reported in ref. 8, are included in this figure with a green straight line. The explicit solvent results are the only ones consistent with the experiments.

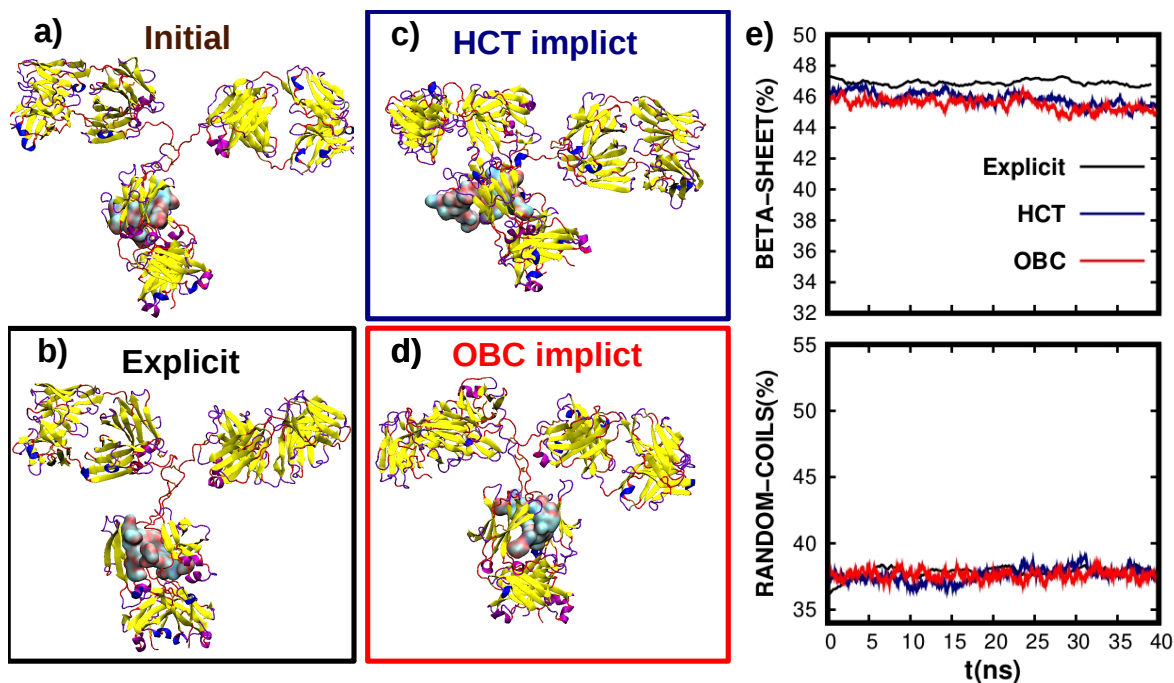


Figure S5: **Simulation of the dynamic of the free IgG solvated in water.** a) Initial configuration of the IgG protein. The color representation used for the protein is the same as in Fig. 1 of the main manuscript. b)-d) Final configurations obtained after 40 ns of MD simulation of the free IgG protein solvated in water using b) Explicit TIP3P,⁵ c) HCT implicit⁶ and d) OBC implicit⁴ solvent methods. e) Time evolution of the β -sheet (top) and random-coils (bottom) content of the IgG during that MD simulation using the three solvent methods here considered: Explicit⁵ (black), HCT implicit⁶ (blue) and OBC implicit⁴ (red).

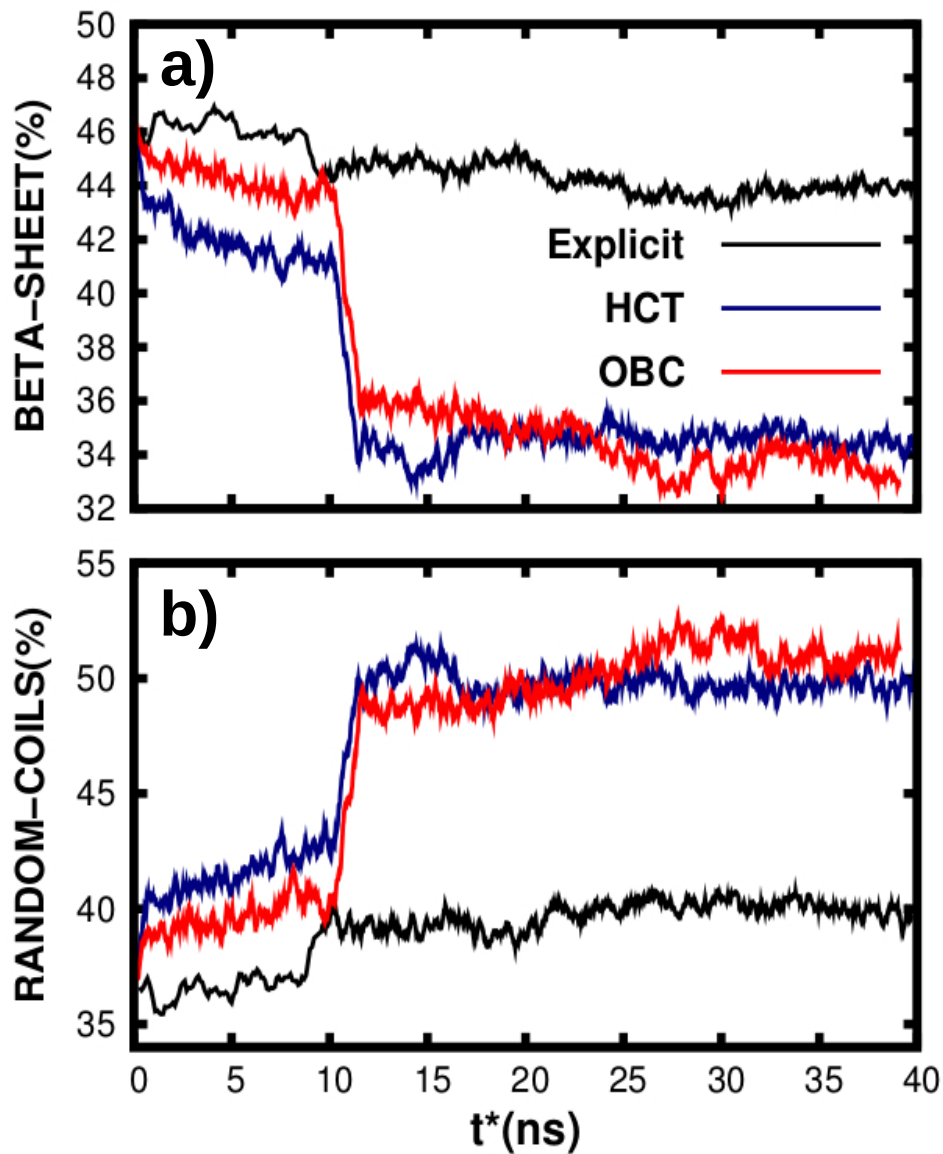


Figure S6: Time evolution of the secondary structure content of the IgG during the adsorption process. We show the time evolution of the a) β -sheet and b) random-coils content using the three solvent methods here considered: Explicit⁵ (black), HCT implicit⁶ (blue) and OBC implicit⁴ (red).

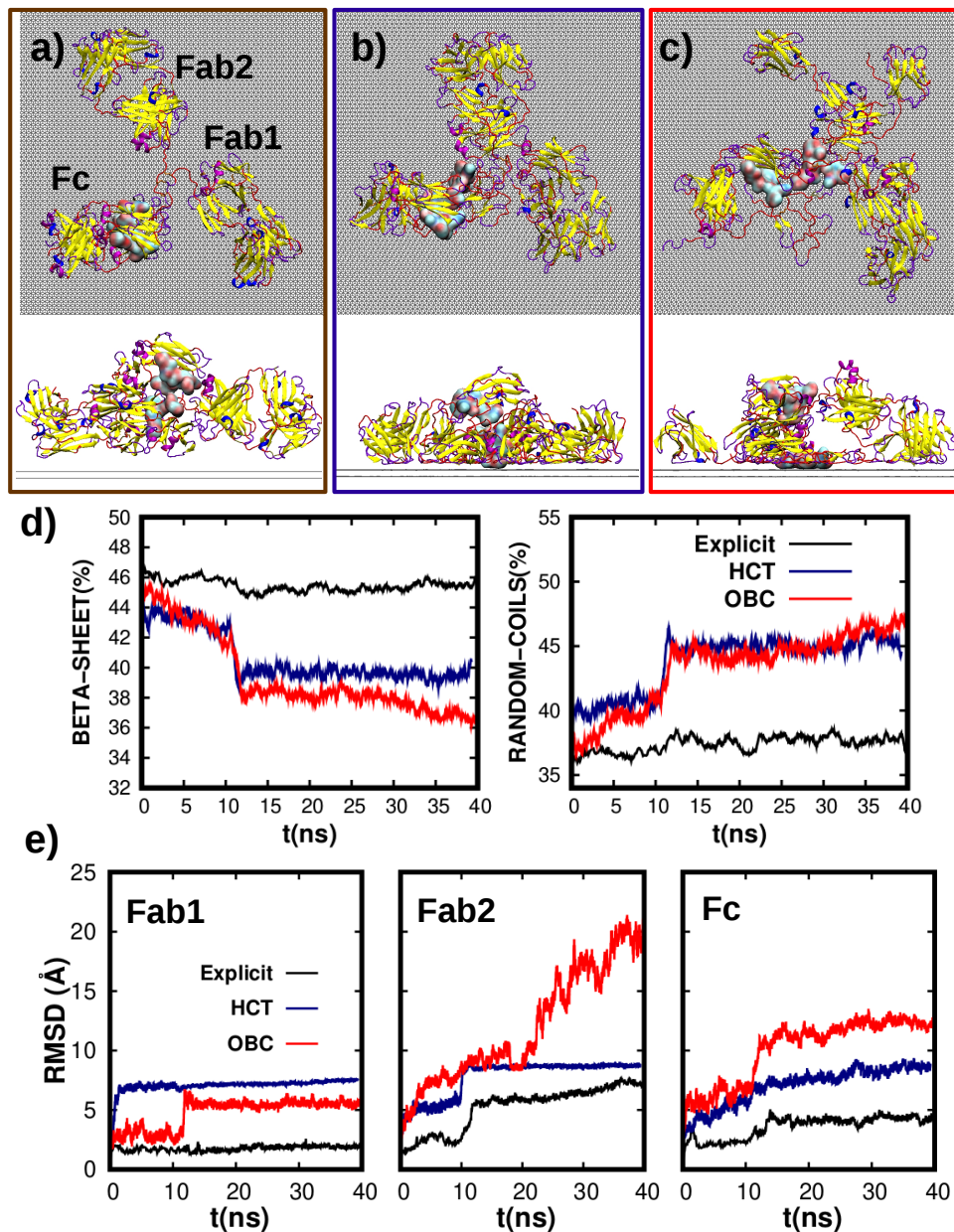


Figure S7: Simulation of the IgG adsorption process using implicit solvation methods starting from a different IgG orientation in the surface (flat-180x-flipped). a) Initial configuration of the IgG protein. Both top (first row) and side views (second row) are here shown. The color representation used for the protein is the same as in Fig. 1 of the main manuscript. b)-c) Final configurations obtained after 40 ns of adsorption MD simulation using b) HCT implicit⁶ and c) OBC implicit⁴ solvation methods. Both top (first row) and side views (second row) are shown. The configuration obtained using explicit solvent is reported in the Supporting Material of ref. 8. d) Time evolution of the β -sheet (left) and random-coils (right) content of the IgG during that adsorption simulation using Explicit (black), HCT implicit⁶ (blue) and OBC implicit⁴ (red) solvation methods. e) Time evolution of the RMSD for the atoms belonging to each IgG fragment, i.e. Fab1, Fab2 and Fc, using Explicit (black), HCT implicit⁶ (blue) and OBC implicit⁴ (red) solvation methods. The time of simulation for the explicit solvent case has been rescaled in all the figures using the relation $t^* = t_{sim}/4.6$.

2.3.2 Effect of the non-electrostatic solvation contribution ($\Delta E_{SOL(nonel)}$) in the adsorption process

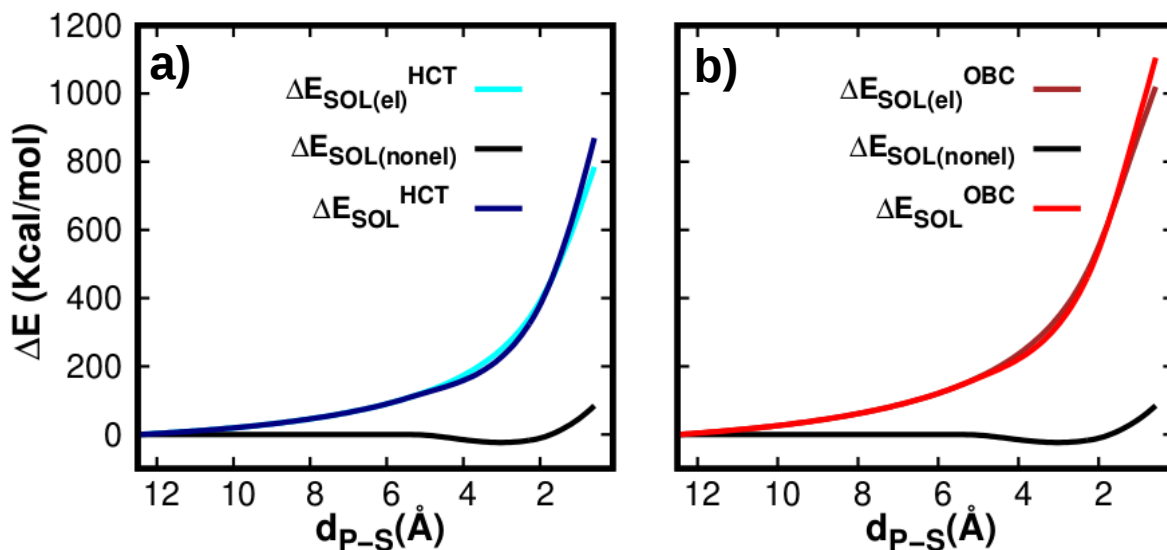


Figure S8: Change of the total solvation energy, E_{SOL} , of the protein+substrate system with the distance between them (d_{P-S}). Here the results obtained using the a)HCT⁶ and b)OBC⁴ implicit solvent methods are showed. Its two energy components, $E_{SOL(nonel)}$ y $E_{SOL(el)}$ are also showed. From this figure it can be observed that the OBC implicit solvent method predicts a larger increase of E_{SOL} when the protein approaches to the surface than the HCT implicit solvent method.

2.3.3 vdW interaction: the cost of breaking the solvation shell and its importance

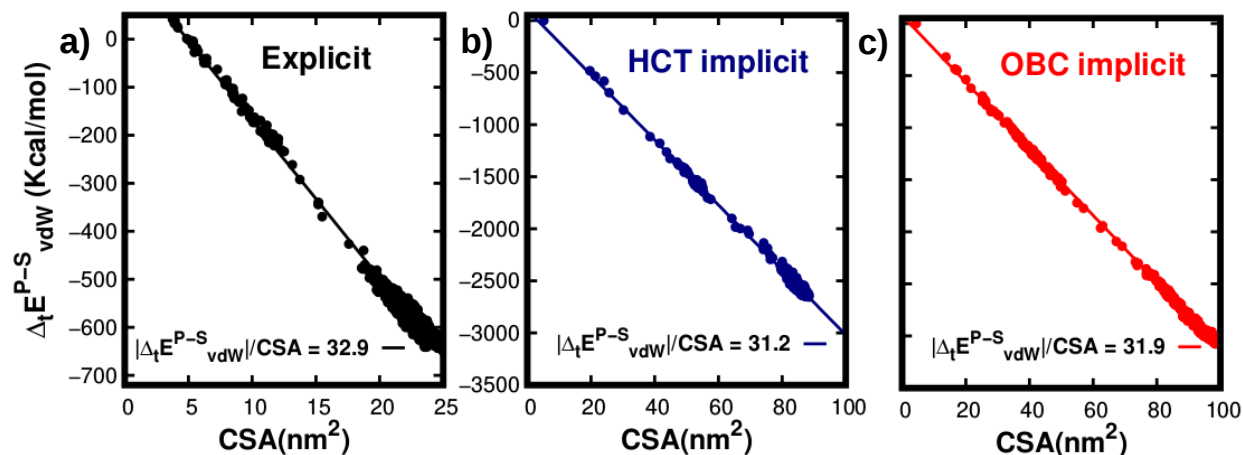


Figure S9: Evolution of the interaction energy between the protein and the substrate, E_{vdW}^{P-S} with the contact surface area (CSA). Here we show the results obtained using the three solvent methods considered in this work: **a)**Explicit⁵ (black), **b)**HCT implicit⁶ (blue) and **c)**OBC implicit⁴ (red). In the three cases, the rate of change of E_{vdW}^{P-S} with the CSA is shown. That rate of change has been computed via a linear regression of the MD data.

2.3.4 Electrostatic interaction: implicit solvent simulation does not correctly shield the internal energy of the protein adsorbed

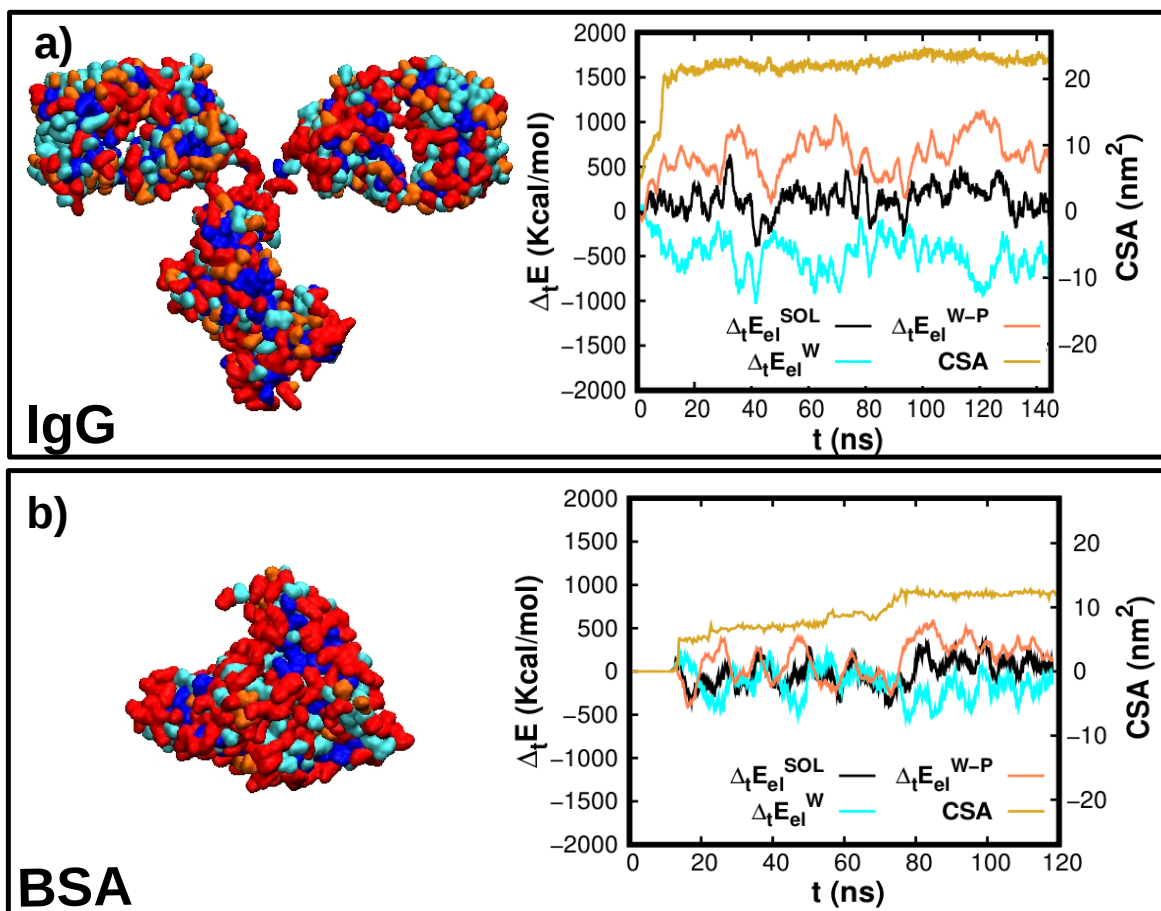


Figure S10: **Comparison of the evolution of the solvation electrostatic contribution during the IgG adsorption and the BSA adsorption.** Evolution of the electrostatic contribution to the solvation energy (E_{el}^{SOL} , in black) using explicit solvent⁵ during the adsorption process on a graphene surface of **a)** the IgG protein **b)** the BSA protein (simulations performed in ref. 9). The evolution of the CSA (yellow) and the two non-null energy components to E_{el}^{SOL} (E_{el}^W in cyan and E_{el}^{W-P} in orange) are also shown. For both cases is also included a representation of the two proteins according to the hydrophobicity index of its residues: very hydrophobic (blue), hydrophobic (cyan), neutral (orange), and hydrophilic (red).

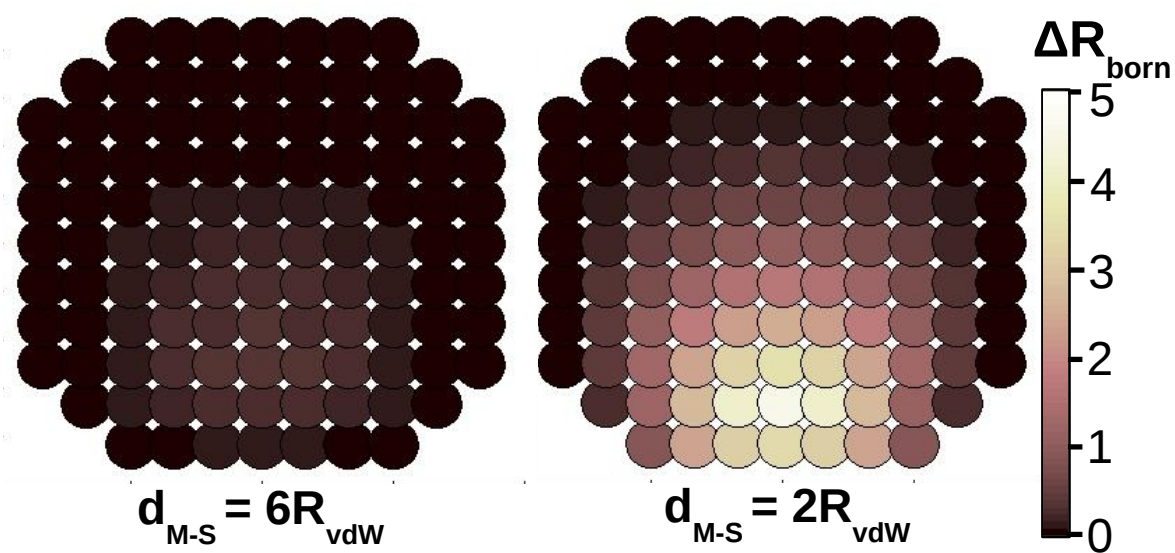


Figure S11: Modeling the loss of the solvent electrostatical screening predicted by **implicit solvent methods**. Change of the Born radii (R_{born})⁶ per sphere while decreasing the distance between the model molecule and the model surface (d_{M-S}). The results obtained when $d_{M-S} = 6 R_{vdW}$ (left) and $d_{M-S} = 2 R_{vdW}$ (right) are here shown.

References

- (1) Berendsen, H. J. C.; Postma, J. P. M.; van Gunsteren, W. F.; DiNola, A.; Haak, J. R. Molecular dynamics with coupling to an external bath. *The Journal of Chemical Physics* **1984**, *81*, 3684–3690.
- (2) Allen, M. P.; Tildesley, D. J. *Computer simulation of liquids*, 2nd ed.; Oxford University Press, 2017.
- (3) Rogge, S.; Vanduyfhuys, L.; Ghysels, A.; Waroquier, M.; Verstraelen, T.; Maurin, G.; Van Speybroeck, V. A Comparison of Barostats for the Mechanical Characterization of MetalOrganic Frameworks. *Journal of Chemical Theory and Computation* **2015**, *11*, 5583–5597.
- (4) Onufriev, A.; Bashford, D.; Case, D. A. Exploring Protein Native States and Large-Scale Conformational Changes With a Modified Generalized Born Model. *Proteins* **2004**, 383 – 394.
- (5) Jorgensen, W. L.; Chandrasekhar, J.; Madura, J. D.; Impey, R. W.; Klein, M. L. Comparison of Simple Potential Functions for Simulating Liquid Water. *J. Chem. Phys.* **1983**, *79*, 926–935.
- (6) Hawkins, G. D.; Cramer, C. J.; Truhlar, D. G. Parametrized Models of Aqueous Free Energies of Solvation Based on Pairwise Descreening of Solute Atomic Charges From a Dielectric Medium. *J. Phys. Chem.* **1996**, 19824 – 19839.
- (7) Harris, L. J.; Larson, S. B.; Hasel, K. W.; McPherson, A. Refined Structure of an Intact IgG2a Monoclonal Antibody. *Biochemistry* **1997**, *36*, 1581 – 1597.
- (8) Vilhena, J. G.; Dumitru, A. C.; Herruzo, E. T.; Mendieta-Moreno, J. I.; Garcia, R.; Serena, P. A.; Perez, R. Adsorption Orientations and Immunological Recognition of Antibodies on Graphene. *Nanoscale* **2016**, *8*, 13463–13475.

- (9) Vilhena, J. G.; Rubio-Pereda, P.; Vellosillo, P.; Serena, P. A.; Pérez, R. Albumin (BSA) Adsorption over Graphene in Aqueous Environment: Influence of Orientation, Adsorption Protocol, and Solvent Treatment. *Langmuir* **2016**, *32*, 1742–1755.